Research Article

Tiange Zhang, Meirong Ren, Jifeng Cui, Xiaogang Chen*, and Yidan Wang

Electroosmotic flow for Eyring fluid with Navier slip boundary condition under high zeta potential in a parallel microchannel

https://doi.org/10.1515/phys-2022-0018
received January 07, 2022; accepted February 24, 2022

Abstract: The electroosmotic flow of non-Newtonian fluid–Eyring fluid in microparallel pipes under high zeta potential driven by the combination of pressure and electric force is studied. Without using the Debye–Hückel (DH) linear approximation, the numerical solutions of the fluid potential distribution and velocity distribution obtained using the finite difference method are compared with the analytical approximate solutions obtained using the DH linear approximation. The results show that the numerical method in this article is effectively reliable. In addition, the influence of various physical parameters on the electroosmotic flow is discussed in detail, and it is obtained that the velocity distribution of the Eyring fluid increases with the increase in the electric potential under the high zeta potential.

Keywords: high zeta potential, Eyring fluid, Navier slip boundary condition, electroosmotic flow, parallel microchannel

1 Introduction

With the rapid growth of microfluidic technology, related applications have been promoted, for instance chemical analysis, medical diagnosis, *etc.*, [1,2], so a variety of microfluidic devices appear, and the electroosmotic flow (EOF) has received more and more attention. EOF is a kind of fluid flow caused by voltage applied at both ends of porous media, microchannels, and other fluid pipes. Uematsu and Araki [3,4] discussed the adsorption and hydrodynamic effects of polymers near the wall. Most of the early studies on EOF were for Newtonian fluids. But microfluidic equipment is sometimes used to resolve biological fluids, for instance lymph, colloidal suspension, *etc.*, which are non-Newtonian fluids. So it is of great theoretical and practical significance to research EOF of various types of non-Newtonian fluids, such as power-law fluid [5,6], Oldroyd-B fluid [7], Phan–Thien–Tanner fluid [8], generalized Maxwell fluid [9,10], third-grade fluid [11], and so on.

In the abovementioned studies, the electrostatic potential distribution is mostly achieved through solving the Poisson–Boltzmann (PB) equation and using the Debye–Hückel (DH) linear approximation, which is only applicable to the low zeta potential (*i.e.*, $\zeta \leq 25$ mV) [12]. However, in actual application, zeta potentials up to 100–200 mV are often encountered, so it is of great significance to research the EOF for non-Newtonian fluids with high zeta potential without imposing DH linear approximation, many scholars have done a lot of research on these problems. For example, based on the central difference scheme, Nekoubin [13] investigated the EOF for the power-law fluid through a curved rectangular microchannel under high zeta potential without imposing DH linear approximation; by directly solving the nonlinear PB equation, Xie and Jian [14] discussed rotating EOF for power-law fluid with high zeta potential at microchannels; Jiménez *et al.* [15] discussed the start-up of remaining EOF for the Maxwell fluid at asymmetric high zeta potentials on the wall in rectangular microchannels; and so on.

It can be obtained from the above references that different constitutive relations are used for the EOF of different non-Newtonian fluids. However, is there a non-Newtonian fluid model that can be used to describe the EOF in microchannels or nanotubes? Eyring deduced the hyperbolic sine relationship between shear rate and shear stress in 1936 [16], namely Eyring fluid, indicating that Eyring fluid is a non-Newtonian fluid. Yang [17]

* **Corresponding author: Xiaogang Chen,** College of Science, Inner Mongolia University of Technology, Hohhot 010051, China, e-mail: xiaogang_chen@imut.edu.cn
Tiange Zhang, Meirong Ren, Jifeng Cui, Yidan Wang: College of Science, Inner Mongolia University of Technology, Hohhot 010051, China

analyzed the flow of Eyring fluid in nanotubes by using continuum mechanics, and the results showed that Eyring fluid can be used to study nano-scale fluid flow. The problem of slip boundary conditions is also very important in the study of heat transfer and flow characteristics of micro-nano fluids in microchannels, and their behaviors are different in the macro-scale and micro-scale. As we all know, no-slip boundary conditions are widely used in macroscopic fluid flow problems, Zhu and Granick [18] concluded that for micro-nano-scale flows, the no-slip boundary condition may fail, depending on the roughness of the interface and the interface interaction between the solid and the fluid. Therefore, it is necessary to consider the slip boundary conditions when analyzing the flow in the microchannel. Navier first proposed the slip boundary condition, which is given by the linear relationship between slip velocity and wall shear rate. Later, some scholars developed different slip boundary conditions [19]; however, the Navier slip boundary condition is the easiest one and the most proverbially utilized one. For instance, Tan and Liu [20] explored the characteristics of EOF for the Eyring fluid under Navier slip boundary condition in circular microtubes; by utilizing the numerical method, Song *et al.* [21], investigated the rotating EOF for third-grade fluids at parallel plate microchannels under Navier slip boundary conditions; Tan *et al.* [22] discussed EOF for the Eyring fluid under Navier slip boundary conditions in narrow microchannels; Jiang and Qi [23] analyzed the EOF for Eyring fluid at parallel microchannels with Navier slip boundary condition under the combined action of applied electric field force and pressure; Afonso *et al.* [24] proposed under the effect of the Navier slip boundary condition, an analytical solution for mixed pressure-driven electrokinetic slip flows of viscoelastic fluids in hydrophobic microchannels; Jamaati *et al.* [25] presented an analytical solution for pressure-driven electrokinetic flows in planar microchannels with velocity slip at the walls; Soong *et al.* [26] studied an analysis of pressure-driven electrokinetic flows in hydrophobic microchannels with emphasis on the slip effects under coupling of interfacial electric and fluid slippage phenomena. In previous studies, Navier slip boundary conditions have been applied to predict some flow phenomena in carbon nanotubes [27].

Motivated by the above, in this article, we will study the EOF of a non-Newtonian fluid-Eyring fluid in parallel microchannels under high zeta potential under Navier slip boundary conditions, derive the numerical solution of the velocity distribution, and use graphics for numerical discussion.

2 Mathematical model and its solution

We consider a steady EOF for incompressible Eyring fluid at a parallel microchannel in Figure 1, where the width, length, and height of the microchannel are W, L, and $2H$, respectively, and satisfy $L, W \gg 2H$. The channel walls are evenly charged to a zeta potential ψ_w, and the Eyring fluid flows with the combined action of a constant pressure gradient P and an external direct current (DC) electric field E_x applied along the x-direction. The physical and electrical properties of the fluid are considered to be constant. In the light of the symmetry of geometry, only the top half of the micropipe is discussed, *i.e.*, $0 \le y \le H$, and the form of velocity distribution is $\boldsymbol{V} = (v_x(y), 0, 0)$.

Neglecting the influence of gravity on the EOF, Eyring fluid satisfies the Cauchy momentum equation [22],

$$\frac{\mathrm{d}\tau_{yx}}{\mathrm{d}y} + \rho_e E_x = \frac{\partial P}{\partial x}, \tag{1}$$

where $\rho_e E_x$ represents an electric field force per unit volume, and ρ_e is the net charge density. E_x is the applied external electric field, and P is the pressure.

The constitutive relation of Eyring fluid is [16,28]:

$$\tau_{yx} = \tau_0 \operatorname{arcsinh}\left(\frac{1}{\dot{\gamma}_0}\frac{\mathrm{d}v_x}{\mathrm{d}y}\right), \tag{2}$$

where τ_{yx} is the shear stress, τ_0 is a constant with the dimension of stress, $\dot{\gamma}_0$ is a function of temperature with the dimension of the shear rate, τ_0 and $\dot{\gamma}_0$ are the rheological parameters. For small shear stress ($\tau_{yx} \ll \tau_0$), and $\tau_0/\dot{\gamma}_0$ represents the viscosity of the material [17].

From electrostatic theory, the electrostatic potential ψ satisfies the Poisson equation:

$$\frac{\mathrm{d}^2\psi}{\mathrm{d}y^2} = -\frac{\rho_e}{\varepsilon}, \tag{3}$$

Then, the net charge density distribution is

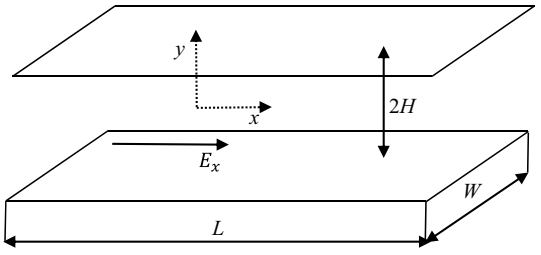

Figure 1: Diagrammatic sketch of flow in the parallel micropipe.

$$\rho_e = -2n_0 ze \sinh\left(\frac{ze\psi}{k_b T}\right), \tag{4}$$

where ε is the dielectric constant, n_0 is the volume concentration of the ions, T is the absolute temperature, z represents the valence of the ions, k_b represents the Boltzmann constant, and e is the unit electronic charge.

Combining Eqs. (4) and (3), the electrostatic potential distribution ψ is given by following nonlinear PB equation:

$$\frac{d^2\psi}{dy^2} = \frac{2n_0 z_0 e}{\varepsilon} \sinh\left(\frac{z_0 e\psi}{k_b T}\right). \tag{5}$$

The potential distribution meets the boundary conditions [22],

$$\left.\frac{d\psi}{dy}\right|_{y=0} = 0, \tag{6}$$

$$\psi(y = H) = \psi_w. \tag{7}$$

Combining Eqs. (4) and (1), Cauchy momentum Eq. (1) can be written as:

$$\frac{d\tau_{yx}}{dy} - 2n_0 ze \sinh\left(\frac{ze\psi}{k_b T}\right) E_x = \frac{\partial P}{\partial x}. \tag{8}$$

The velocity distribution satisfies the following Navier slip boundary condition [17] and symmetry boundary condition,

$$v_x(y = H) = -L_s^0 \left.\frac{dv_x}{dy}\right|_{y=H}, \tag{9}$$

$$\left.\frac{dv_x}{dy}\right|_{y=0} = 0, \tag{10}$$

where L_s^0 is the constant slip length.

Considering the symmetry boundary condition (10) and integrating Eq. (8) from 0 to y, the shear stress τ_{yx} can be deduced:

$$\tau_{yx} = 2n_0 ze E_x \int_0^y \sinh\left(\frac{ze\psi}{k_b T}\right) dy + \frac{\partial P}{\partial x} y. \tag{11}$$

Moreover, we can deduce the following ordinary differential equation for the velocity distribution by using Eqs. (2) and (11)

$$\frac{dv_x}{dy} = \dot{\gamma}_0 \sinh\left(\frac{2n_0 ze E_x}{\tau_0} \int_0^y \sinh\left(\frac{ze\psi}{k_b T}\right) dy + \frac{\partial P}{\partial x}\frac{y}{\tau_0}\right). \tag{12}$$

For the convenience of calculation, this article cites the approximate method of ref. [22], the following approximate expression of hyperbolic sine function is used [29]:

$$\sinh u \approx \begin{cases} u, & 0 < u \le 1, \\ \frac{1}{2}e^u, & u > 1. \end{cases} \tag{13}$$

Such an approximation is mathematically amenable and successfully used in previous studies to obtain the approximate solutions for different problems [29]. In practical applications, such as elastohydrodynamic lubrication, τ_0 is usually very large [30]. Therefore, $2n_0 ze E_x < \tau_0$ is reasonably assumed in this article.

Introducing dimensionless variables

$$\begin{aligned} &\bar{\psi} = \frac{ze}{k_b T}\psi,\ \bar{\psi}_w = \frac{ze}{k_b T}\psi_w,\ \bar{v}_x = \frac{v_x}{V_s},\ \bar{y} = \frac{y}{H}, \\ &\kappa H = \frac{H}{\kappa^{-1}},\ b = L_s^0/H, \end{aligned} \tag{14}$$

here $V_s = -\frac{\varepsilon E_x \psi_w \dot{\gamma}_0}{\tau_0}$ is the Smoluchowski velocity [22]; $\kappa^2 = (2n_0 z^2 e^2)/(\varepsilon k_b T)$ is the DH parameter, where κ^{-1} is called Debye length, which is the characteristic thickness of the electric double layer and d is the dimensionless slip length. For small shear stress ($\tau_{yx} \ll \tau_0$), under certain other conditions, as the viscosity $\tau_0/\dot{\gamma}_0$ decreases, V_s increases, and the dimensionless velocity v_x/V_s decreases.

Substituting Eq. (14) into Eqs. (5)–(7), the PB equation and the boundary conditions for the electrostatic potential distribution take the following dimensionless forms:

$$\frac{d^2\bar{\psi}}{d\bar{y}^2} = (\kappa H)^2 \sinh(\bar{\psi}), \tag{15}$$

$$\left.\frac{d\bar{\psi}}{d\bar{y}}\right|_{\bar{y}=0} = 0, \tag{16}$$

$$\bar{\psi}(\bar{y} = 1) = \bar{\psi}_w. \tag{17}$$

Applying finite difference method (step size 0.02) for the Eqs. (15)–(17), we can obtain numerical solutions of the dimensionless electrostatic potential distribution.

Furthermore, nondimensionalizing the Eqs. (9) and (12) *via* Eq. (14), the nondimensional forms for velocity distribution and the Navier slip boundary condition after some simplification are:

$$\frac{d\bar{v}_x}{d\bar{y}} = -\frac{(\kappa H)^2}{\bar{\psi}_w} \int_0^{\bar{y}} \sinh(\bar{\psi}) d\bar{y} + \Gamma\bar{y}, \tag{18}$$

$$\bar{v}_x(\bar{y} = 1) = -b \left.\frac{d\bar{v}_x}{d\bar{y}}\right|_{\bar{y}=1}. \tag{19}$$

where $\Gamma = -\frac{H^2}{\varepsilon E_x \psi_w}\frac{\partial P}{\partial x}$ is the ratio of pressure to electroosmotic driving force [24].

Integrating Eq. (18) with respect to $\bar{y}$ from $\bar{y}$ to 1 with nondimensional Navier slip boundary condition (19), Eq. (18) for the nondimensional velocity distribution becomes:

$$\bar{v}_x(\bar{y}) = \frac{(\kappa H)^2}{\bar{\psi}_w}\int_{\bar{y}}^{1}\int_{0}^{\bar{y}}\int_{0}^{\bar{y}} \sinh(\bar{\psi})\mathrm{d}\bar{y}\mathrm{d}\bar{y} - \frac{1}{2}\Gamma + \frac{1}{2}\Gamma\bar{y}^2 + \bar{v}_x(1), \tag{20}$$

where $\bar{v}_x(\bar{y}=1) = b\frac{(\kappa H)^2}{\bar{\psi}_w}\int_0^1 \sinh(\bar{\psi})\mathrm{d}\bar{y} - \Gamma b$.

Because there are two variables $\bar{y}$, it is easy to confuse. According to the property of integral, changing the integral variable will not affect the integral result. Therefore, a variable $\bar{y}$ in Eq. (20) is changed to α, the results are as follows

$$\bar{v}_x(\bar{y}) = \frac{(\kappa H)^2}{\bar{\psi}_w}\int_{\bar{y}}^{1}\int_{0}^{\alpha} \sinh(\bar{\psi})\mathrm{d}\alpha\mathrm{d}\bar{y} - \frac{1}{2}\Gamma + \frac{1}{2}\Gamma\bar{y}^2 + b\frac{(\kappa H)^2}{\bar{\psi}_w}\int_0^1 \sinh(\bar{\psi})\mathrm{d}\bar{y} - \Gamma b. \tag{21}$$

Also, integrating Eq. (21) with respect to $\bar{y}$ from 0 to 1, the average velocity is given by

$$\bar{V} = \frac{(\kappa H)^2}{\bar{\psi}_w}\int_0^1\int_{\bar{y}}^{1}\int_{0}^{\alpha} \sinh(\bar{\psi})\mathrm{d}\alpha\mathrm{d}\bar{y}\mathrm{d}\bar{y} + b\frac{(\kappa H)^2}{\bar{\psi}_w}\int_0^1\int_0^1 \sinh(\bar{\psi})\mathrm{d}\bar{y}\mathrm{d}\bar{y} - \Gamma b - \frac{1}{3}\Gamma. \tag{22}$$

By applying numerical integration method (complex trapezoidal formulation, with a step size of 0.02) for Eqs. (21) and (22), we can give approximations about the velocity distribution and the average velocity.

In order to verify the reliability of solutions in this article, under low zeta potential conditions, we will compare the velocity distribution for Eyring fluid with the analytical approximate solution obtained by using the DH linear approximation [23], namely

$$v_x(y) = -\dot{\gamma}_0\int_y^H \sinh\left(\frac{\varepsilon\kappa E_x\psi_w}{\tau_0}\frac{\sinh(\kappa y)}{\cosh(\kappa H)} + \frac{\partial P}{\partial x}\frac{\kappa y}{\kappa\tau_0}\right)\mathrm{d}y - \dot{\gamma}_0 L_s^0 \sinh\left(\frac{\varepsilon\kappa E_x\psi_w}{\tau_0}\frac{\sinh(\kappa H)}{\cosh(\kappa H)} + \frac{\partial P}{\partial x}\frac{\kappa H}{\kappa\tau_0}\right). \tag{23}$$

3 Results and discussion

In this part, we will study the influence of zeta potential, ratio Γ of pressure to electroosmotic driving force, characteristic thickness κ^{-1} of electrical double layer, and dimensionless slip length b to the velocity of Eyring fluid. To this end, we choose the dielectric constant $\varepsilon = 6.95 \times 10^{-10}$ C^2 N^{-1} m^{-2}, the wall zeta potential $\psi_w = -50$ mV, the applied electric field $E_x = 500$ V m^{-1}, the rheological parameter $\tau_0 = 43.4$ N m^{-2} [31], the half microchannel height $H = 3.04$ μm, and the constant slip length $L_s^0 \sim 1$ nm to 10 μm [26].

Figure 2 shows the comparison of numerical solution (21) and analytical approximate solution (23) of Eyring fluid velocity distribution under low zeta potential $\bar{\psi}_w = 1$. It is noted that they match very well, so the numerical method used in this article is reliable.

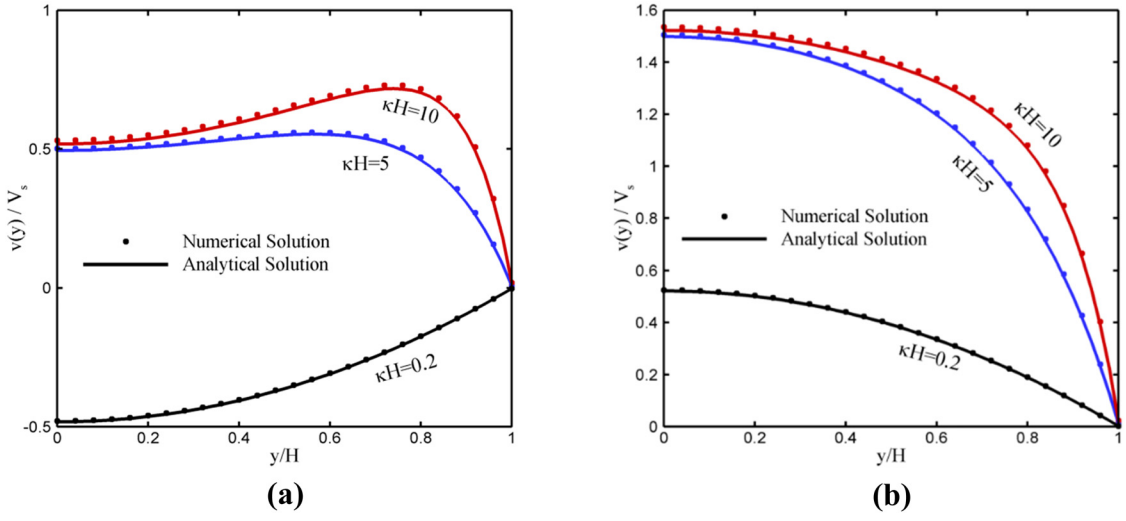

Figure 2: Comparison between the numerical solution and DH analytical approximate solution of the velocity at different κH, when (a) $\Gamma = 1$, $b = 0.002$ and (b) $\Gamma = -1$, $b = 0.002$.

Figures 3 and 4 illustrate the effect of the ratio Γ of pressure to electroosmotic driving force for the velocity profile at high zeta potential. It can be seen from the figure that the dimensionless velocity enhances with the increase in the zeta potential $\bar{\psi}_w$ and decreases with the increase in Γ, respectively, for $\kappa H = 30$, $b = 1/4$ and $\kappa H = 0.4$, $b = 1/4$. when $\Gamma < 0$, it promotes fluid flow; this is because the pressure field and the electric field generate the driving force in the same direction, thus promoting the fluid flow. Conversely, when $\Gamma > 0$, the opposite phenomenon occurs, which hinders fluid flow.

Figure 5 displays the change in trends of the velocity distribution with the characteristic thickness κ^{-1} of the electric double layer at high zeta potential. The dimensionless velocity enhances with the increase in the zeta potential $\bar{\psi}_w$ when other conditions are the same. With the slip boundary condition, the velocity on the channel wall is not zero. It shows that the dimensionless velocity profile exhibits a plug-like profile and increases with the increase in κH for the same Γ when the value of H and b are fixed and $\kappa H > 1$, which is consistent with the previous experimental results [17], and exhibits a parabolic-like profile when $0 < \kappa H < 1$. Furthermore, for $0 < \kappa H < 1$, the dimensionless velocity enhances with the increase in κH for $\Gamma \leq 0$, and the absolute value of dimensionless velocity decrease as κH increases for $\Gamma > 0$ (Figure 6).

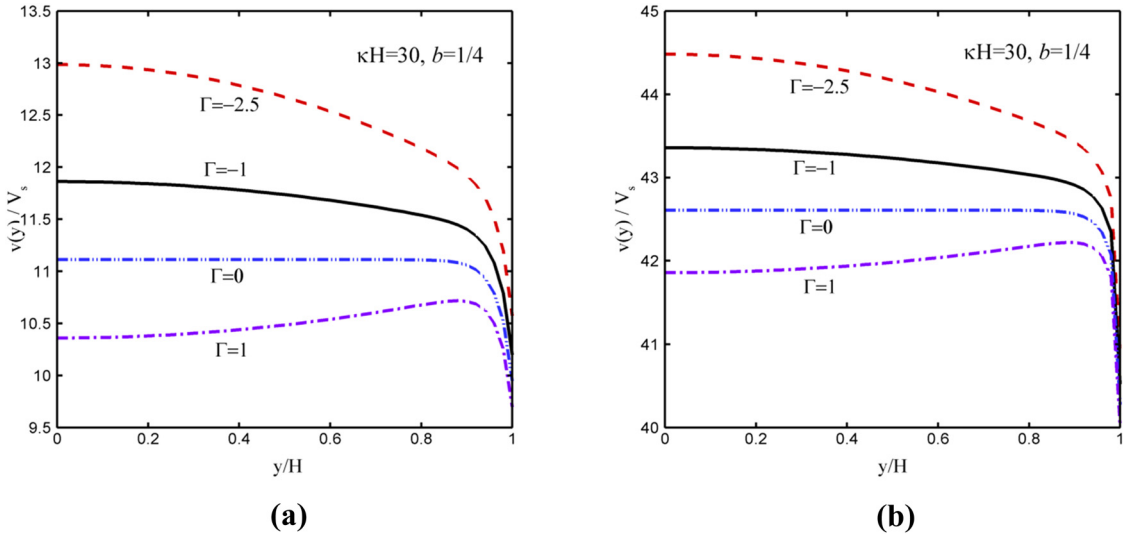

Figure 3: The change in dimensionless velocity distribution for different Γ ($\kappa H = 30$, $b = 1/4$). (a) $\bar{\psi}_w = 2$. (b) $\bar{\psi}_w = 5$.

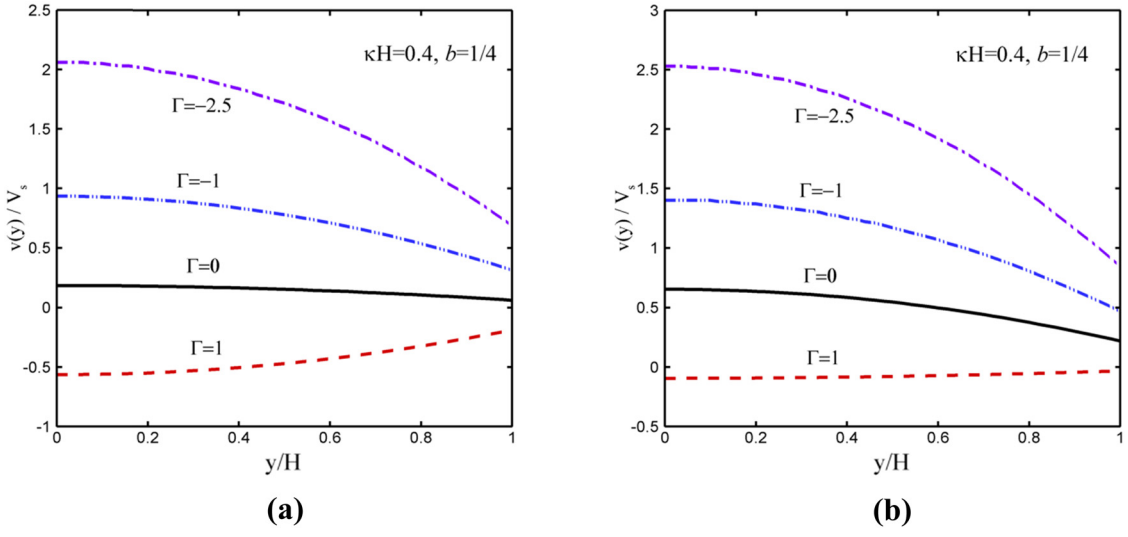

Figure 4: The change in dimensionless velocity distribution for different Γ ($\kappa H = 0.4$, $b = 1/4$). (a) $\bar{\psi}_w = 2$. (b) $\bar{\psi}_w = 5$.

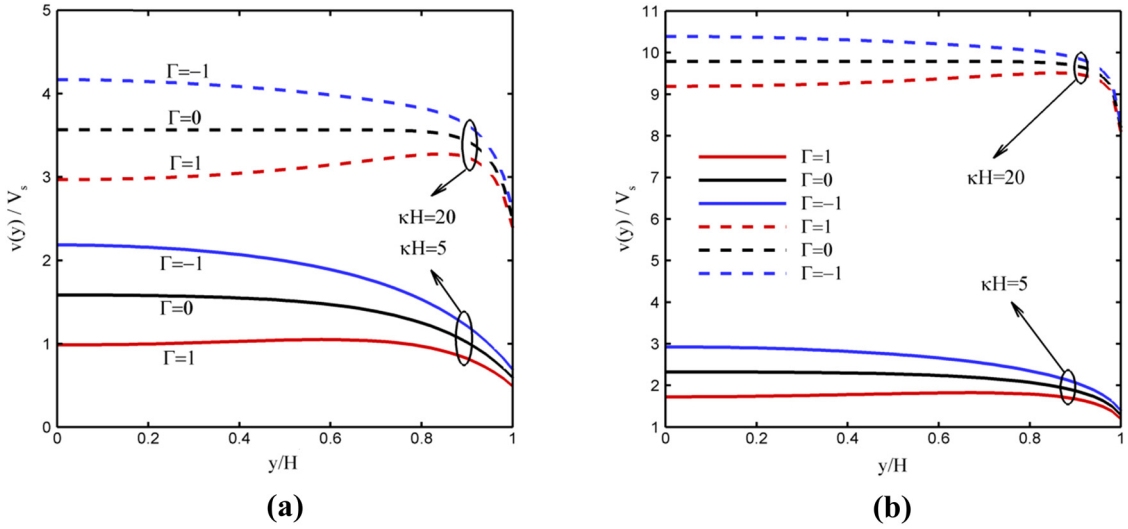

Figure 5: The change in dimensionless velocity distribution for different κ^{-1}, where $b = 0.1$, $\kappa H > 1$. (a) $\bar{\psi}_w = 2$. (b) $\bar{\psi}_w = 5$.

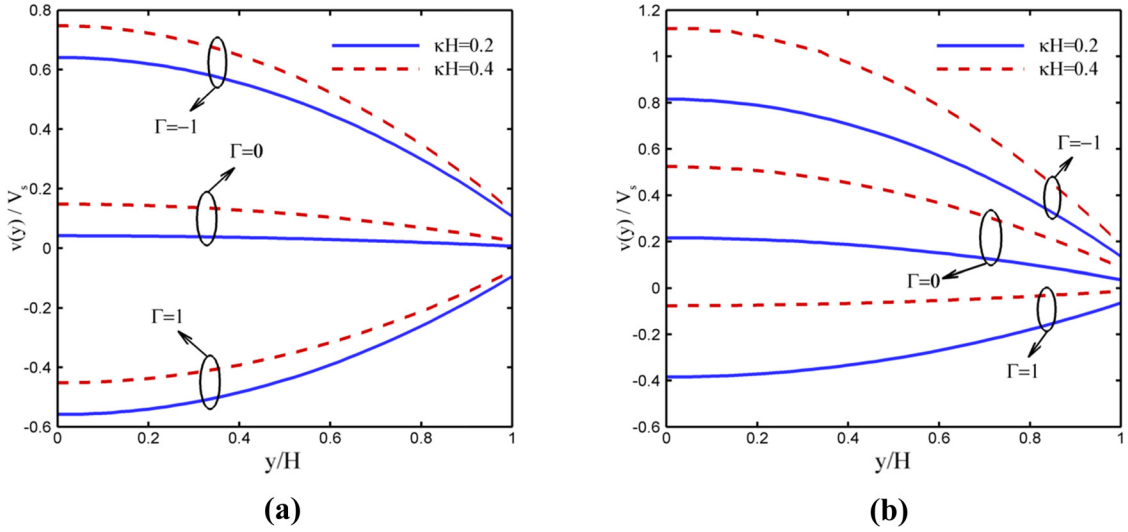

Figure 6: The change in dimensionless velocity distribution for different κ^{-1}, where $b = 0.1$, $\kappa H < 1$. (a) $\bar{\psi}_w = 2$. (b) $\bar{\psi}_w = 5$.

Figure 7 indicates the relationship between the dimensionless average speed and the electric parameter κH for various dimensionless slip lengths. The diagrams show that: the dimensionless velocity increases as zeta potential $\bar{\psi}_w$ increases for different dimensionless slip length values; it can be seen that the average velocity $\bar{V}$ approaches the Smoluchowski velocity V_s when $\kappa H \to \infty$, under the no slip boundary condition. But, when the dimensionless slip length is not zero ($b \neq 0$) and the electrokinetic parameter κH is larger, the average velocity can be several times larger than that for the Newtonian fluid with the no slip boundary condition. Under the same electrokinetic parameter κH, the dimensionless average velocity increases with the increase in b.

Figure 8 represents the relationship between the dimensionless average velocity and the zeta potential $\bar{\psi}_w$ on the wall. It can be seen from the figure that the distribution of fluid velocity increases as the zeta potential $\bar{\psi}_w$ of the wall increases. It is because the high zeta potential can generate greater electric field force and pressure near the EDL area. It shows that the dimensionless velocity profile exhibits a plug-like profile when $\kappa H > 1$, and exhibits a parabolic-like profile when $0 < \kappa H < 1$.

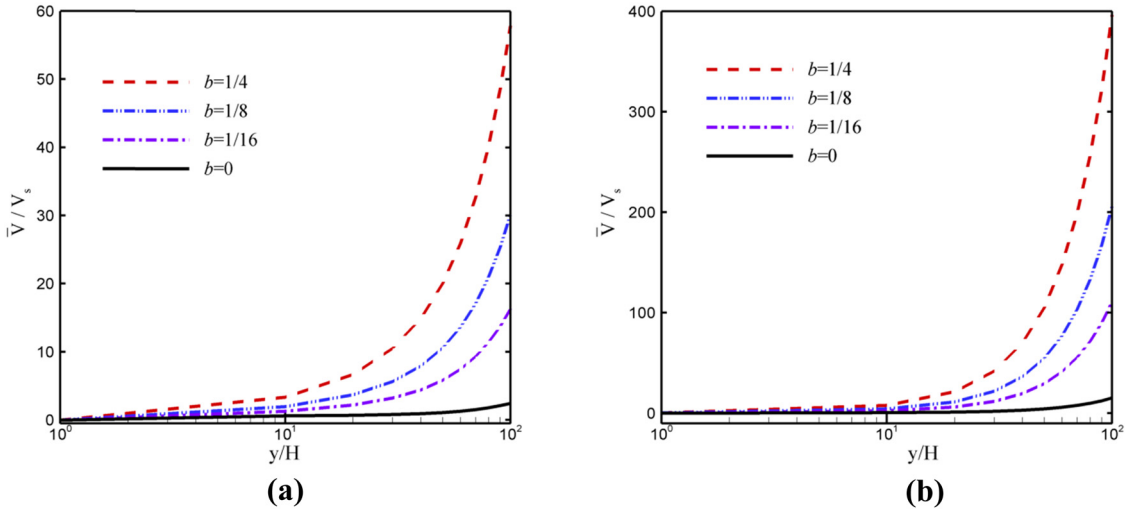

Figure 7: The influence of different values of b on the dimensionless velocity distribution, where $\Gamma = 1$. (a) $\bar{\psi}_w = 2$. (b) $\bar{\psi}_w = 5$.

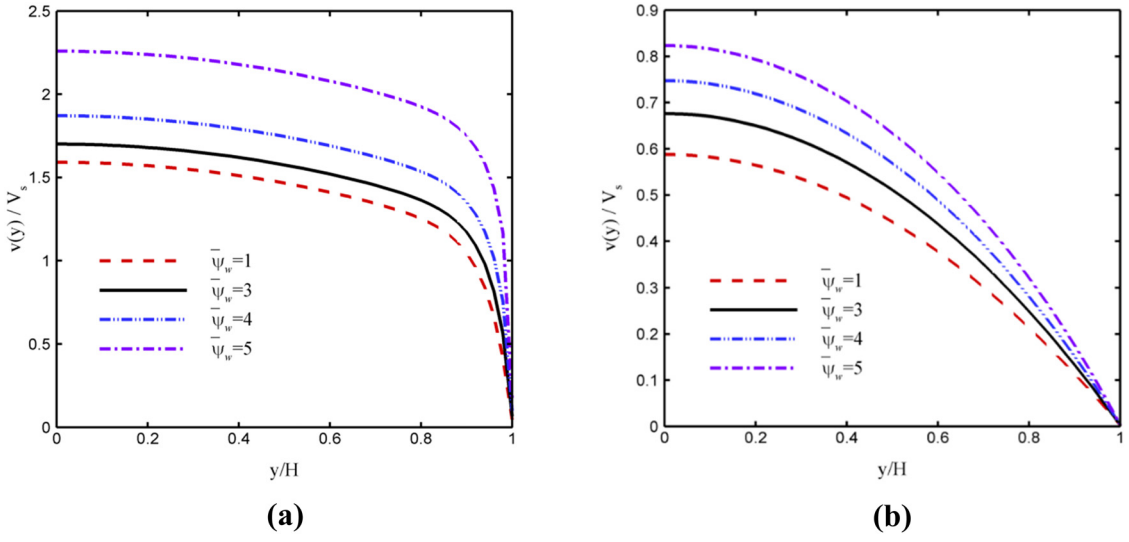

Figure 8: The influence of different values of $\bar{\psi}_w$ on the dimensionless velocity distribution, where (a) $\kappa H = 20$, $\Gamma = -1$, $b = 0.002$ and (b) $\kappa H = 0.4$, $\Gamma = -1$, $b = 0.002$.

To compare the EOF of Eyring fluid with other fluids in the microchannel, Figure 9 shows the comparison of Eyring fluid and Newtonian fluid ($n = 1$). The exact solution of the power-law fluid velocity is given by Zhao *et al.* [32]. When the behavior index of the power-law fluid is $n = 1$, the result is a Newtonian fluid. It can be seen from the figure that the Eyring fluid has a higher velocity than the Newtonian fluid ($n = 1$). In addition, Eyring fluids are easier and faster to be driven than Newtonian fluid in microchannels. Therefore, Eyring fluid can be better used to study the flow phenomenon in carbon nanotubes [27].

4 Conclusion

The EOF for Eyring fluid under Navier slip boundary condition at high zeta potential is discussed under the combined action of applied electric field force and pressure at a parallel microchannel in this work. The electrostatic potential distribution and velocity distribution of the fluid are given by the finite difference method, and the influences of relevant physical parameters for the velocity are studied. The results show that the relationship between the dimensionless velocity distribution and the electrokinetic parameter κH is nonlinear. The velocity

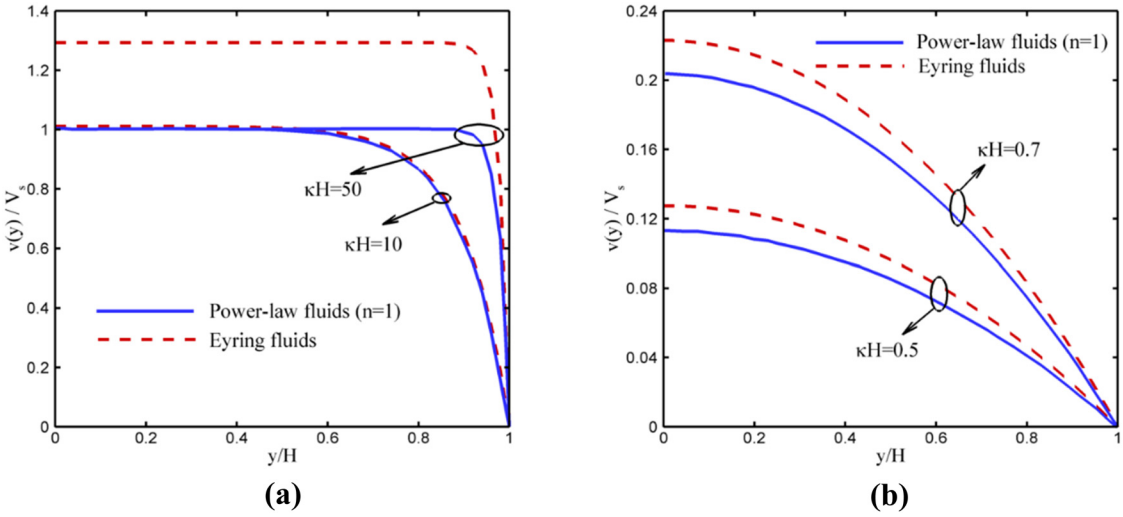

Figure 9: Comparison of the velocity distribution of Eyring fluids and Newtonian fluids (*i.e.*, $n = 1$), where $\bar{\psi}_w = 1$, $\Gamma = 0$, $b = 0$. (a) $\kappa H > 1$. (b) $\kappa H < 1$.

profile of the Eyring fluid exhibits a plug-like profile at high values of κH. In addition, increasing the values of κH can remarkably improve the average velocity; increasing the values of $\bar{\psi}_w$ can improve the velocity distribution significantly.

Funding information: The authors wish to express their sincere appreciation to the National Natural Science Foundation of China (12062018), the Natural Science Foundation of Inner Mongolia (2020MS01015) and the Colleges and Universities Youth Science and Technology Talent Support Program Funded Project of Inner Mongolia Autonomous Region (NJYT22075).

Author contributions: All authors have accepted responsibility for the entire content of this manuscript and approved its submission.

Conflict of interest: The authors state no conflict of interest.

References

[1] Zhao C, Yang C. Electrokinetics of non-Newtonian fluids: a review. Adv Colloid Interface. 2013;201(4):94–108.
[2] Li DQ. Encyclopedia of microfluidics and nanofluidics. Vol. 778. US: Springer; 2008. p. 948–54.
[3] Uematsu Y. Nonlinear electro-osmosis of dilute non-adsorbing polymer solutions with low ionic strength. Soft matter. 2015;11(37):7402–11.
[4] Uematsu Y, Araki T. Electro-osmotic flow of semidilute polyelectrolyte solutions. J Chem Phys. 2013;139(9):9265.
[5] Bhadri S. Electroosmotic flow of a power law fluid in an elliptic microchannel. Colloid Surface A. 2016;492:144–51.
[6] Baños RD, Arcos JC, Bautista O, Méndez F, Merchán CEA. Mass transport by an oscillatory electroosmotic flow of power-law fluids in hydrophobic slit microchannels. J Braz Soc Mech Sci. 2021;43(1):1–15.
[7] Liang P, Wang S, Zhao M. Numerical study of rotating electroosmotic flow of Oldroyd-B fluid in a microchannel with slip boundary condition. Chinese J Phys. 2020;65:459–71.
[8] Sadeghi A, Saidi MH, Mozafari AA. Heat transfer due to electroosmotic flow of viscoelastic fluids in a slit microchannel. Int J Heat Mass Tran. 2011;54(17):4069–77.
[9] Li XX, Yin Z, Jian YJ, Chang L, Su J, Liu QS. Transient electro-osmotic flow of generalized Maxwell fluids through a microchannel. J Non-Newton Fluid. 2012;187:43–7.
[10] Wang S, Zhao M, Li X. Transient electro-osmotic flow of generalized Maxwell fluids in a straight pipe of circular cross section. Cent Eur J Phys. 2014;12(6):445–51.
[11] Mamata P, Sudarsan P. Electro-osmotic flow of a third-grade fluid past a channel having stretching walls. Nonlinear Engineering. 2019;8(1):56–64.
[12] Levine S, Marriott JR, Neale GH, Epstein N. Theory of electrokinetic flow in fine cylindrical capillaries at high zeta-potentials. J Colloid Interf Sci. 1975;52(1):136–49.
[13] Nekoubin N. Electroosmotic flow of power-law fluids in curved rectangular microchannel with high zeta potentials. J Non-Newton Fluid. 2018;260:54–68.
[14] Xie ZY, Jian YJ. Rotating electroosmotic flow of power-law fluids at high zeta potentials. Colloid Surface A. 2014;461(1):231–9.
[15] Jiménez E, Escandón J, Méndez OB. Start-up electroosmotic flow of Maxwell fluids in a rectangular microchannel with high zeta potentials. J Non-Newton Fluid. 2016;227(37):17–29.
[16] Eyring H. Viscosity, plasticity, and diffusion as examples of absolute reaction rates. J chem phys. 1936;4(4):283–91.

[17] Yang FQ. Flow behavior of an Eyring fluid in a nanotube: the effect of the slip boundary condition. Appl Phys Lett. 2007;90(13):133105-1.
[18] Zhu YX, Granick S. Limits of the hydrodynamic no-slip boundary condition. Phys Rev Lett. 2002;88(10):1061021–4.
[19] Thompson PA, Troian SM. A general boundary condition for liquid flow at solid surfaces. Nature. 1997;63(6649):360–2.
[20] Tan Z, Liu J. Electro-osmotic flow of Eyring fluids in a circular microtube with Navier's slip boundary condition. Phys Lett A. 2017;381(32):2573–7.
[21] Song J, Wang S, Zhao M, Li N. Numerical study on the rotating electro-osmotic flow of third grade fluid with slip boundary condition. Z Naturforschung A. 2020;75(7):649–55.
[22] Tan Z, Qi HT, Jiang XY. Electroosmotic flow of Eyring fluid in slit microchannel with slip boundary condition. Appl Math Mechanics. 2014;35(006):689–96.
[23] Jiang YT, Qi HT. Electro-osmotic slip flow of Eyring fluid in a slit microchannel. Acta Physica Sin-Ch Ed. 2015;64(17):222–7.
[24] Afonso AM, Ferrás LL, Nóbrega JM, Alves MA, Pinho FT. Pressure-driven electrokinetic slip flows of viscoelastic fluids in hydrophobic microchannels. Microfluid Nanofluid. 2014;16(6):1131–42.
[25] Jamaati J, Niazmand H, Renksizbulut M. Pressure-driven electrokinetic slip-flow in planar microchannels. Int J Therm Sci. 2010;49:1165–74.
[26] Soong CY, Hwang PW, Wang JC. Analysis of pressure-driven electrokinetic flows in hydrophobic microchannels with slip-dependent zeta potential. Microfluid Nanofluid. 2010;9:211–23.
[27] Holt JK, Park HG, Wang Y, Stadermann M, Artyukhin AB, Grigoropoulos CP, et al. Fast mass transport through sub-2-nanometer carbon nanotubes. Science. 2006;312(5776):1034–7.
[28] Bird RB, Armstrong R, Hassager O. Dynamics of Polymeric Liquids. Vol. 649. New York: John Wiley and Sons; 1987. p. 169–253.
[29] Philip JR, Wooding RA. Solution of the Poisson–Boltzmann equation about a cylindrical particle. J Chem Phys. 1970;52(2):953–9.
[30] Liu XL, Jiang M, Yang P, Kaneta M. Non-Newtonian thermal analyses of point EHL contacts using the Eyring model. J Tribol. 2005;127:70–81.
[31] Bosse MA, Araya H, Troncoso SA, Arce PE. Batch electrophoretic cells with Eyring fluids: analysis of the hydrodynamics. Electrophoresis. 2002;23(14):2149–56.
[32] Zhao C, Zholkovskij E, Masliyah JH, Yang C. Analysis of electroosmotic flow of power-law fluids in a slit microchannel. J Colloid Interf Sci. 2009;326(2):503–10.